



Impact of the Chinese Spring Festival on PM_{2.5} air quality in the Beijing-Tianjin-Hebei and surrounding region: a machine learning-based counterfactual modeling approach

Yuan Li¹, Qili Dai^{1,5}, Wubin Zhu¹, Xuan Liu¹, Jiandong Shen², Renchang Yan², Yunshan Li¹, Jing Ding³, Young Su Lee⁴, Yufen Zhang¹, and Yinchang Feng¹

¹Key Laboratory of Urban Air Particulate Pollution Prevention and Control of Ministry of Ecology and Environment, College of Environmental Science and Engineering, Nankai University, Tianjin 300350, China

²Hangzhou Ecological Environment Monitoring Center, Hangzhou 310007, China

³Tianjin Environmental Meteorological Center, Qixiangtai Road, Tianjin 300074, China

⁴Department of Environment and Energy, Sejong University, 209 Neungdong-ro, Gwangjin-gu, Seoul 05006, Republic of Korea

⁵Tianjin Key Laboratory of Software Experience and Human Computer Interaction, Tianjin 300457, China

Correspondence: Qili Dai (daiql@nankai.edu.cn) and Yinchang Feng (fengyc@nankai.edu.cn)

Received: 16 September 2025 – Discussion started: 13 October 2025

Revised: 12 March 2026 – Accepted: 28 March 2026 – Published: 23 April 2026

Abstract. Acute short-term exposure to extremely high PM_{2.5} levels posed serious health risks. Human culture-based festival activities can significantly alter emission patterns, often leading to sharp yet understudied fluctuations in air quality. The Chinese Spring Festival (CSF), marked by large-scale family reunions and widespread use of fireworks, raises air pollution concerns. Commonly, this effect is quantified using receptor models or chemical transport models, but the relevant chemical component data and emission inventories are often lacking. This study presents a machine learning counterfactual approach to quantify PM_{2.5} changes associated with holiday activities. The results align well with traditional chemical composition-based estimates of fireworks contributions, highlighting the strong potential of using widely accessible routine monitoring data to quantify source contributions driven by specific interventions. Applied to 28 major cities in the Beijing-Tianjin-Hebei and surrounding region, one of the most polluted areas in China, the approach revealed an average PM_{2.5} reduction of $19.0 \pm 17.5 \mu\text{g m}^{-3}$ during the full 2025 CSF holiday period. Despite this regional mean decrease, short-lived but extremely high PM_{2.5} peaks were observed in several cities during the peak fireworks window, with fireworks contributing $\geq 35\%$ of first-day severe PM_{2.5} deterioration and up to 89% in the city of Baoding. This approach offers a robust tool for evaluating holiday emissions and guiding air quality interventions.

1 Introduction

Fine particulate matter (PM_{2.5}) pollution remains a major global environmental issue, adversely affecting visibility, air quality, human health, and climate change (Pui et al., 2014; Pye et al., 2021; Yang et al., 2020). Although annual mean PM_{2.5} concentrations in major economies such as the USA,

Europe and China have significantly declined over the past decades (Li et al., 2023), severe air pollution events characterized by high PM_{2.5} concentrations still occur frequently in many regions especially during cold seasons in the Northern Hemisphere (Yin et al., 2019). These events pose a substantial short-term exposure risk to human health. In addition to the unfavorable meteorological conditions during au-

tumn and winter lead to the accumulation of pollutants, aperiodic elevation of source emissions (e.g., natural dust storm, biomass burning, and wildfire) can also cause poor PM_{2.5} air quality. Understanding the causes and sources of short-term air pollution events is crucial for informing emergency mitigation policies aimed at protecting the public from high exposure risks.

Cultural events that associated with changes in economic activities and human social behavior patterns often shape air quality as well (Hua et al., 2021; Huang et al., 2024; Wei et al., 2022). Among which, the Chinese Spring Festival (CSF), the most significant traditional festival in Chinese culture, is featured by increased indoor family gatherings, reduced road traffic, and celebratory activities such as fireworks and firecrackers. During this period, a distinct “holiday effect” is observed in air quality variations, often marked by a decline in nitrogen oxide (NO_x) levels and complex changes in PM_{2.5} concentrations (Li et al., 2021; Dai et al., 2021a; Wu et al., 2022). Severe air pollution has been widely observed across Chinese cities during Lunar New Year’s Eve, due to the fireworks emissions (Dai et al., 2021a; Jiang et al., 2015; Lai and Brimblecombe, 2017, 2020). Reported data indicate that on the first day of the 2024 Lunar New Year, hourly PM_{2.5} concentrations exceeded 150 µg m⁻³ in over 250 cities across China (<https://www.cenews.com.cn/media-article.html?aid=26801&mediaID=1732>, last access: 31 March 2026). In 66 of these cities, concentrations surpassed 500 µg m⁻³, while in 10 cities they exceeded 1000 µg m⁻³. Such extremely high PM_{2.5} levels raised serious concerns about the short-term health risks associated with acute exposure. Traditionally, identifying and apportioning festival-related sources of PM_{2.5} (e.g., fireworks emissions) has primarily relied on aerosol chemical composition data for receptor modeling or emission inventory data for chemical transport models (Gao et al., 2018; Tian et al., 2014; Zhou et al., 2022). However, such data are often lacking in many cities, where there is an urgent need to evaluate such a holiday effect. Dai et al. (2021a) estimated changes in the emission strengths of air pollutants during the CSF holiday period in major Chinese cities by decoupling meteorological influences from their ambient concentrations, but our understanding of air quality changes attributable to the CSF – especially regarding shifts in emission strengths – remains inadequate due to the absence of effective evaluation approaches.

Machine learning (ML) has been popular for inferring causal-effect relations from observational data across many fields (Han et al., 2022; Leist et al., 2022; Prospero et al., 2020). In this work, we develop an ML-based counterfactual modeling framework that is causally informed but not intended to identify strict causal effects, and that quantifies changes in PM_{2.5} air quality and emission strength associated with short-term interventions such as the CSF under a *business-as-usual* (BAU) scenario (Fig. 1). The approach involves training ML models on data excluding the intervention period to simulate air quality under a counterfac-

tual BAU emissions scenario, thereby isolating the impact of short-term interventions. We first employed an ML-based regression model to predict the counterfactual, unobservable PM_{2.5} levels under the assumption that the CSF did not occur. Both factual and counterfactual PM_{2.5} levels were then re-predicted under average meteorological conditions during the study period to adjust for time-varying meteorological fluctuations, thereby revealing changes in emission strength. Differences between the real observations and the modeled counterfactual levels were attributed to the impact of the CSF holiday. Using in-situ measurement data from Hangzhou, China, the ML modeled CSF holiday effect was validated against PM_{2.5} source contributions estimated via dispersion normalized positive matrix factorization (DN-PMF) based on continuous online measurements of PM_{2.5} chemical composition. The validated approach was then applied to quantify the changes in both PM_{2.5} emission strength and ambient air quality attributable to the CSF in a key region of Northern China (Beijing-Tianjin and the surrounding 26 major cities), which experienced severe air pollution in past decade as well as the 2025 holiday period. Our study aims to provide a simple and efficient evaluation framework that is broadly applicable for assessing air quality intervention policies.

2 Data and methods

2.1 Data sources

The PM_{2.5} chemical composition data were obtained from the Wolongqiao Automatic Particulate Matter Monitoring Station in Hangzhou, Zhejiang Province, located within the Hangzhou Flower Nursery (30.2456° N, 120.1269° E) in the Xihu District downtown area. The dataset covers the period from 20 December 2023 to 20 February 2024, and includes measurements of carbonaceous components (organic carbon, OC, and elemental carbon, EC), water-soluble ions (NO₃⁻, SO₄²⁻, NH₄⁺, Mg²⁺), and trace elements (Fe, K, Cl, Ca, Zn, Pb, Mn, Si, Cu, As, Cr, V, Ba, Ni). The analytical instruments/methods, method detection limits (MDLs), and uncertainty (error fractions) for these PM_{2.5} chemical species used as PMF inputs are summarized in Table S1 in the Supplement. Organic carbon (OC) comprises both primary organic carbon (POC), directly emitted from emission sources, and secondary organic carbon (SOC), formed through atmospheric reactions of gaseous precursors. Following the methodology described by Dai et al. (2018), we applied the minimum OC/EC ratio method to separate OC into POC and SOC. However, because primary emission characteristics may change during the Spring Festival, SOC estimated using the minimum OC/EC ratio (EC-tracer) approach may carry higher uncertainty. We therefore examined the period dependence of (OC/EC)_{min} by calculating the 10th-percentile OC/EC ratio separately for the periods before and after Lunar New Year’s Eve (pre-eve: 3.10; post-eve: 3.13; full period: 3.10). The deduced EC-tracer-based

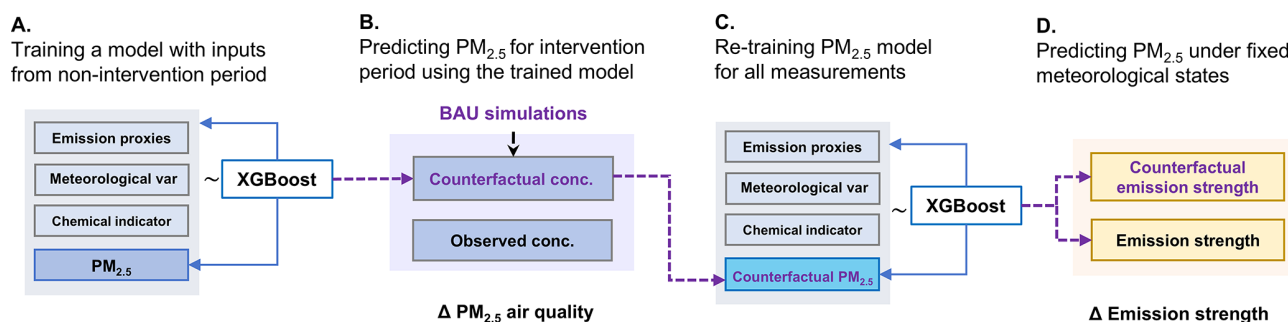


Figure 1. The flowchart includes four major steps: (A) PM_{2.5} air quality modeling based on the non-intervention period, (B) counterfactual prediction of PM_{2.5} concentrations for the intervention period using the pre-trained model, (C) re-training PM_{2.5} air quality model for all measurements using factual and counterfactual PM_{2.5} data, and (D) predicting PM_{2.5} under fixed meteorological conditions. Differences between observed PM_{2.5} and modeled counterfactual levels are the holiday-attributable air quality changes. Correspondingly, differences between meteorology-fixed PM_{2.5} for factual and counterfactual scenarios are the holiday-attributable emission changes.

SOC is included as an input variable in the PMF analysis to help represent the secondary organic component. Nevertheless, potential non-stationarity of primary emissions during the Spring Festival may introduce additional uncertainty, and related results are interpreted with caution.

Hourly air pollutant data were collected from the China National Environmental Monitoring Center (CNEMC) data sharing platform (available at <https://quotsoft.net/air/>, last access: 31 March 2026) for Hangzhou, using the average PM_{2.5} concentration from ground-based observations at all national monitoring stations in Hangzhou. This study focuses on the “2 + 26” cities designated by the Chinese government for intensive air pollution control, including Beijing, Tianjin, and 26 major cities in the surrounding provinces of Hebei, Henan, Shandong, and Shanxi. Thus, hourly PM_{2.5} concentrations were also downloaded for the “2 + 26” cities.

The meteorological data for each of the studied cities, as shown in Table S2, were obtained from the ERA5 dataset, the fifth-generation global climate atmospheric reanalysis product provided by the European Centre for Medium-Range Weather Forecasts (ECMWF). Based on the Hybrid Single-Particle Lagrangian Integrated Trajectory Model (HYSPLIT), 72 h backward air mass trajectory analysis was conducted at 100 m a.g.l. (Hou et al., 2022). This analysis classified high-altitude air masses into six trajectory clusters, representing distinct regional pollutant origins, with trajectory lengths indicating transport distances (i.e., the spatial range of external pollutant contributions to the local area). These regional transport variables, together with local meteorological conditions, atmospheric photochemical oxidants (O_x, NO₂+O₃), and temporal predictors, were subsequently incorporated into the statistical modeling of ambient air pollutant concentrations. More details are provided in Sect. S1, where preprocessing of the downloaded ERA5 meteorological variables is described, and in Sect. S2, where the representativeness of the ERA5 meteorological data is evaluated.

2.2 ML-Based counterfactual PM_{2.5} air quality predictions for the CSF under BAU emission scenario

To predict the ambient PM_{2.5} concentrations during the overnight pollution period (from 9–10 February 2024) without the influence of the CSF-related emission changes, we first employed the XGBoost algorithm, chosen for its superior fitting accuracy, to train on data from non-pollution periods (i.e., periods without interventions) in the original dataset. The trained PM_{2.5} model was then used to predict the counterfactual PM_{2.5} concentrations during the pollution period with inputs of observed meteorological and temporal variables, simulating an air quality under BAU emission scenario (Han et al., 2022). The differences between observed PM_{2.5} concentrations and predicted counterfactual PM_{2.5} levels during pollution periods represent the ‘holiday effect’ on air quality (Fig. 1). When the entire CSF period is defined as the intervention period, the overall impact of the Spring Festival on air pollution can also be assessed accordingly. The modeling incorporated temporal variables (Unix time for linear trends, day of the year for annual and seasonal cycles, day of the week for weekly patterns, hour of the day for diurnal variations, and lunar calendar day for festival-related emissions, as suggested by existing literature (e.g., Dai et al., 2021a, 2023), meteorological parameters (wind speed/direction, temperature, relative humidity, surface pressure, mixing layer height, total cloud cover, solar radiation, precipitation), chemical variables, and backward air mass trajectories with lengths to quantify regional transport influences – all of which align with the variables required for subsequent meteorological normalization. In the XGBoost modeling process, 80 % of the data was allocated for training and 20 % for testing. Model hyperparameters were optimized using Bayesian optimization (Optuna, version 4.5.0), with a 5-fold cross-validation strategy on the training set. The detailed model configuration and settings are provided in Sect. S3, where the corresponding learning curve analysis

(Fig. S1), the ML model predictive uncertainty (Fig. S2), and the SHAP summary plots (Fig. S3) are also discussed. The code and data used for this study are available in Zenodo (Li, 2026; see also the Code and data availability section).

It is important to note that the CSF constitutes a composite intervention that involves multiple simultaneous behavioral and emission changes. These include fireworks emissions, reductions in traffic activity, and adjustments in industrial or construction operations. Because of this complexity, the key identification assumptions required for strict causal inference cannot be fully validated in this setting. Examples include the assumptions of conditional independence, adequate covariate overlap between treated and untreated periods, and the absence of confounding between the intervention and the covariates. In particular, calendar-related variables such as the lunar-day index are inherently tied to the intervention and therefore cannot be treated as independent adjustment covariates. Given these considerations, the proposed framework is not intended to provide a structural causal estimate. Instead, we adopt a causally informed counterfactual modeling perspective that focuses on estimating the deviation of observed PM_{2.5} from a machine-learning-based BAU scenario. This framing maintains conceptual consistency with the data-generating process and allows the analysis to remain rigorous without overstating causal claims.

2.3 ML-Based meteorology-fixed PM_{2.5} prediction technique

Changes in air pollutant emission strengths can be estimated by decoupling the meteorological variability from observed air pollutant time series (Ding et al., 2023), which can be achieved by a ML-based meteorological normalization technique (Dai et al., 2023; Grange et al., 2018; Shi et al., 2021; Vu et al., 2019). The method assumes that the ambient PM_{2.5} concentration $X_i(t)$ in city i is a function of both the emission intensity $E_i(t)$ and meteorological conditions $M_i(t)$ [including local meteorology, regional transport meteorology, and chemistry]:

$$X_i(t) = f\{E_i(t), M_i(t)\} + \varepsilon_i(t) \quad (1)$$

where $\varepsilon_i(t)$ is the residual term. A tree-based random forest algorithm was commonly employed to train the model using observational data. Time-related variables were selected to capture periodic variations in emissions and atmospheric processes. The selected time-related variables include Unix time (seconds since 1 January 1970, 00:00:00 UTC), day of the year, day of the week, hour of the day, and lunar calendar day to incorporate the influence of traditional festivals on emission patterns. Meteorological parameters such as wind speed, wind direction, temperature, relative humidity, surface pressure, mixing layer height, total cloud cover, surface net solar radiation, and precipitation were also included. Additionally, backward air mass trajectories and their

lengths were added to indicate potential regional transport influences. The model f , describing the relationship between PM_{2.5} concentration, emissions, and meteorological conditions, is expressed as:

$$f\{E_i(t), M_i(t)\} = E\{X_i(t) | E_i(t), M_i(t)\} \quad (2)$$

To smooth the meteorologically-induced “noise” in observations, the PM_{2.5} concentration contributed at time t was adjusted by selecting N sets of consistent meteorological variables from the training dataset and reconstructing a new explanatory dataset (replacing the original meteorological variables). The model f was then applied to predict the pollutant concentration under these N consistent meteorological conditions, and the arithmetic mean of these predictions was taken as the adjusted concentration $X_i(t)_{\text{adj}}$ under fixed meteorological conditions, as demonstrated in Dai et al. (2026):

$$X_i(t)_{\text{adj}} = \frac{1}{N} \sum_{n=0}^N f_{t,n} \quad (3)$$

We applied meteorology-fixed prediction technique to adjust both the observed PM_{2.5} concentrations and the predicted counterfactual PM_{2.5} concentrations during the CSF. Differences between the normalized real observed and counterfactual PM_{2.5} are attributed to holiday-related emission strength changes.

2.4 DN-PMF modelling of festival-related source contributions

Based on the principle of chemical mass balance, PMF extracts factors by identifying the covariance (co-variation) of multiple linearly additive observed component variables over time (Dai et al., 2020; Paatero and Tapper, 1994). The measured mass concentration X_{ij} ($\mu\text{g m}^{-3}$) of the j th chemical species in the i th receptor sample can be expressed as:

$$X_{ij} = \sum_{k=1}^p g_{ik} f_{kj} + e_{ij} \quad (4)$$

Where f_{kj} ($\mu\text{g } \mu\text{g}^{-1}$) represents the mass fraction of the j th species in the k th source (constrained to non-negative values), g_{ik} ($\mu\text{g m}^{-3}$) is the contribution concentration of the k th source to the i th receptor sample (also non-negative), p is the number of source categories, and e_{ij} is the residual between the measured and modeled mass concentrations for the ij th sample. The input components include POC, SOC, EC, NO₃⁻, SO₄²⁻, NH₄⁺, K⁺, Cl⁻, Si, Ca, Cr, Mn, Fe, Ni, Cu, Zn, As, and Pb. Uncertainties associated with the input data were set following the approach of previous work (Brown et al., 2015; Dai et al., 2020). The Dispersion Normalized PMF (DN-PMF) was utilized to reduce the impacts of meteorological dispersion on the source emissions induced covariance (Dai et al., 2020, 2021b; Yang et al., 2022). The chemical component monitoring data and their uncertainty matrices are normalized to the average ventilation coefficient (VC, as

a measure of atmospheric dispersion capacity) over the study period, effectively deconvolving “noise” caused by meteorological dispersion. The dispersion normalized concentration $C_{VC,i}$ for the i th sample is given by:

$$C_{VC,i} = C_i \times \frac{VC_i}{VC_{\text{mean}}} = \frac{C_i \times (\text{MLH}_i \times u_i)}{\frac{1}{m} \sum_{i=1}^m (\text{MLH}_i \times u_i)} \quad (5)$$

where MLH_i is the mixing layer height at the time of the i th sample, and u_i is the ground-level wind speed at that time.

3 Results and discussion

3.1 Source apportionment results of PM_{2.5} for the 2024 CSF haze episode in Hangzhou, China

DN-PMF analysis was applied to the PM_{2.5} chemical composition dataset collected in Hangzhou from 20 December 2023 to 20 February 2024. An optimal nine-factor solution was obtained, with small, normally distributed residuals, demonstrating good model performance (Table S3). The robustness of this solution was further validated through bootstrap diagnostics across solutions with six to ten factors. Specifically, the nine-factor solution exhibited the highest bootstrap mapping stability (96 %–100 %) and no unmapped factors, confirming it as the most stable and interpretable among all tested solutions. Based on diagnostic tracers, chemical profiles, and temporal signatures, the resolved factors were interpreted as coal combustion, fireworks, secondary organic aerosols, biomass burning, fugitive dust, vehicle emissions, industrial sources, secondary nitrate, and secondary sulfate. The factor profiles are shown in Fig. S4. Factor 1 (Coal combustion) is characterized by elevated concentrations of As and Pb, two well-established tracers of coal combustion. EC and OC also contribute moderately, whereas sulfate is present only in minor amounts. This is expected because most atmospheric SO₄²⁻ originates from secondary formation and is therefore assigned predominantly to the secondary sulfate factor rather than the primary coal combustion factor. Factor 2 (Fireworks) shows very high concentrations of K⁺ and Cu. K⁺ is a canonical tracer of pyrotechnic materials, and the marked enrichments of Cu exhibits sharp peaks during New Year’s Eve, closely matching the temporal pattern of firework discharges (Wang et al., 2007, 2024). This strong chemical signature, together with its event-driven temporal behavior, confirms the identification of this factor as fireworks. Factor 3 (Secondary organic aerosols) is strongly dominated by SOC, with more than 80 % of the receptor’s total SOC apportioned to this factor, and shows negligible contributions from primary tracers such as EC or metals. The chemical characteristics and the absence of primary emission markers indicate that this factor represents secondary organic aerosol formation. Factor 4 (Biomass burning) exhibits an overall low mass contribution from EC and POC. Its only clear diagnostic features are the elevated K⁺ and Cl⁻ levels, with 63.5 % of the receptor-site Cl⁻ attributed to this factor. Several metal

species, including Fe, Pb, Cr, Ni, Cu, and Zn, also appear at low concentrations. Although the chemical signature is weak and partially mixed, the combined presence of enriched K⁺ and substantial Cl⁻ still supports the interpretation of this factor as a diluted biomass burning source during the winter period. Factor 5 (Fugitive dust) presents high Ca, Si, and moderate Fe, typical of crustal and mineral dust materials. The abundance of Ca reflects contributions from road dust and resuspended soil particles, confirming its attribution to fugitive dust. Factor 6 (Vehicle emissions) exhibits strong EC and notable Fe and Zn, the latter two being associated with brake wear and tire abrasion (Viana et al., 2008). Moderate OC further supports its assignment to traffic-related emissions. Factor 7 (Industrial sources) is enriched in transition metals including Cr, Mn, Ni, Cu, Zn, and Pb. These elements are characteristic of metallurgical and manufacturing activities, supporting its interpretation as industrial emissions. Factor 8 (Secondary nitrate) is dominated by NO₃⁻ together with NH₄⁺, clearly indicating the formation of secondary inorganic nitrate. Factor 9 (Secondary sulfate) shows extremely high contributions of SO₄²⁻ and NH₄⁺. The dominance of sulfate, formed through oxidation of SO₂ in the atmosphere, identifies this factor as secondary sulfate. DISP uncertainty diagnostics for the nine-factor solution showed narrow confidence intervals and no evidence of factor swapping, confirming the overall stability and robustness of the DN-PMF results. Moreover, the enrichment of specific tracer elements does not necessarily correspond directly to the mass contribution of a given source factor. Within the PMF modeling, tracer species primarily serve as indicators for source identification, whereas factor-resolved mass contributions reflect the overall mixture of chemical species associated with each source profile. In addition, atmospheric particles are often internally mixed, and tracer elements from fireworks emissions may coexist with secondary species such as sulfate or nitrate. Consequently, the enhancement of specific tracer elements should be interpreted primarily as evidence of source influence rather than as a direct proxy for the quantitative mass contribution of that source.

3.2 Changes in air quality and source-specific PM_{2.5} over the 2024 CSF haze episode in Hangzhou

During the haze episode, spanning approximately from 19:00 on 9 February to 19:00 on 10 February, both observed and meteorologically-adjusted PM_{2.5} in Hangzhou increased sharply, with observed levels peaking at 394 μg m⁻³ and meteorologically normalized values reaching a maximum of 123 μg m⁻³ (Fig. S5). Concurrently, SO₂ levels also exhibited a sudden rise. In contrast, NO₂ and CO showed a rapid increase at the onset of the event, followed by a sharp decline. Rather than interpreting these gas-phase patterns as direct evidence of fireworks-related chemical species, we highlight that gas tracers and PM tracers often respond to different source processes and atmospheric lifetimes (Li et al., 2025).

The pronounced decrease in NO₂ and CO more likely reflects the substantial weakening of traffic and combustion-related emissions during the holiday period, rather than the formation of nitrate-rich particles from fireworks. In parallel, O₃ concentrations dropped abruptly and then rebounded, suggesting an O₃ titration effect driven by freshly emitted NO. This behavior further supports the notion that the gaseous species reflect rapid changes in atmospheric chemistry and emission conditions, rather than serving as direct compositional indicators of the fireworks plume. Accordingly, we use NO₂ mainly as an independent corroboration of reduced traffic emissions, while the identification of fireworks contributions relies primarily on the PM_{2.5} chemical fingerprints and the counterfactual analysis. In terms of meteorological conditions, the pollution evolution was accompanied by unfavorable meteorological conditions for dispersion over the night (low VC, see Fig. S5). Figure 2a, b shows the compositional changes in PM_{2.5} during the holiday period. A clear shift in source contributions is observed. The concentrations and proportions of secondary inorganic aerosols, including NO₃⁻ ($-9.7 \mu\text{g m}^{-3}$, -24.6%) and NH₄⁺ ($-4.7 \mu\text{g m}^{-3}$, -12%), decreased markedly relative to the pre-holiday period (5 to 8 February 2024), likely due to reduced industrial and vehicular emissions. In contrast, the concentrations and proportions of fireworks tracers such as K⁺ ($+15 \mu\text{g m}^{-3}$, $+13.6\%$), Cl⁻ ($+5.1 \mu\text{g m}^{-3}$, $+4\%$), Ba ($+1.6 \mu\text{g m}^{-3}$, $+1.5\%$) and Cu ($+0.5 \mu\text{g m}^{-3}$, $+0.5\%$) increased substantially. These enhancements indicate that intensive fireworks and firecracker use became a major contributor to PM_{2.5}, leading to a pronounced change in its chemical profile during the celebration period.

To further substantiate our hypothesis, we conducted an analysis of elemental ratios. During the New Year's Eve haze episode, the K/EC ratio exhibited an abrupt, order-of-magnitude increase, with peak values nearing 13 – more than 60 times higher than the background level (~ 0.2 from 21 January to 8 February 2024; Fig. S6). This sharp deviation from the baseline provides strong evidence for the introduction of a distinct aerosol population characterized by high potassium and low elemental carbon content (“K-rich, EC-poor”). Similarly, the K/Ba ratio showed a pronounced shift, forming a relatively stable low-value plateau during the event (average ~ 10 , coefficient of variation $\sim 16\%$). In contrast, the background period was marked by highly irregular and strongly fluctuating K/Ba ratios (Fig. S7). This transition from chaotic to stable behavior suggests the emergence of a strong, independent source with a comparatively uniform K–Ba composition. Before the fireworks episode, the fluctuating K/Ba ratios were accompanied by consistently low Ba concentrations (average $0.01 \mu\text{g m}^{-3}$) and moderate contributions from the biomass burning factor, as identified by the PMF analysis presented later ($0.74 \mu\text{g m}^{-3}$, 1.6% of PM_{2.5}), indicating that the variability was likely influenced by mixed combustion sources (e.g., biomass burning or residential combustion) rather than fireworks emissions. Consis-

tently, chloride concentrations and the fireworks factor remained low before the event but increased sharply during the fireworks episode, reinforcing the distinction between the pre-holiday variability and the characteristic fireworks signature. This pattern may also be related to a geographical shift in emissions under the influence of the Spring Festival holiday-related activities, when increased rural residential combustion can influence urban air quality through regional transport, as discussed by Li et al. (2025). Taken together, the elemental ratio patterns provide compelling evidence that concentrated firework emissions on New Year's Eve were a substantial contributor to this pollution episode.

Figure 2c, d present the source contributions of the nine factors resolved by DN-PMF and show their temporal variations before, during, and after the New Year's Eve haze episode. The pollution episode over the New Year's Eve was exclusively driven by the sudden increase of the fireworks emissions featuring relatively high K⁺, Cl⁻, Ba, Al and SO₄²⁻, which are major components of black powder in the form of KClO₃ or KNO₃, basic fireworks material of magalium alloy (95% Al and 5% Mg) and oxidizers such as Barium compounds (Ba(NO₃)₂ and BaClO₃) (Dai et al., 2020; Joshi et al., 2019). The maximum concentration of fireworks emissions reached up to $167 \mu\text{g m}^{-3}$ at midnight on New Year's Eve, accounting for 42% of the observed PM_{2.5} by mass. In addition to fireworks emissions, holiday-related source changes also encompass a significant reduction in vehicle emissions (-63%) due to decreased traffic flow, alongside a substantial increase in dust pollution ($+4215\%$) from concentrated firework activities, compared to pre-holiday levels (5 to 8 February 2024). Furthermore, halted industrial production and the shutdown of construction sites, which had already begun near a week prior to the holiday, also reflect changes in emission sources driven by the holiday activities.

Specifically, during the haze period on New Year's Eve 2024 in Hangzhou, the average contributions of PM_{2.5} from nine distinct sources were analyzed, as illustrated in the pie chart in Fig. 2. The primary sources of PM_{2.5}, ranked by their contribution percentages, are as follows: fireworks (76.8%), secondary sulfate (9%), secondary organic aerosols (4.7%), fugitive dust (3.3%), biomass burning (2.6%), coal combustion (2.5%), vehicle emissions (0.6%), secondary nitrate (0.5%), and industrial sources (0.01%). Compared to the period before New Year's Eve, the contribution of the primary PM_{2.5} sources during the haze event on New Year's Eve experienced significant changes. The primary source accounted for approximately 85.7% of the total PM_{2.5}, dominating the composition. In contrast, the average proportion of secondary particulate matter was 14.3%, which was notably lower than that observed before New Year's Eve. During the haze period on New Year's Eve, the concentrated emissions from fireworks led to a dramatic increase in their contribution, with the average concentration of fireworks-related sources surging more than tenfold compared to the same period on the

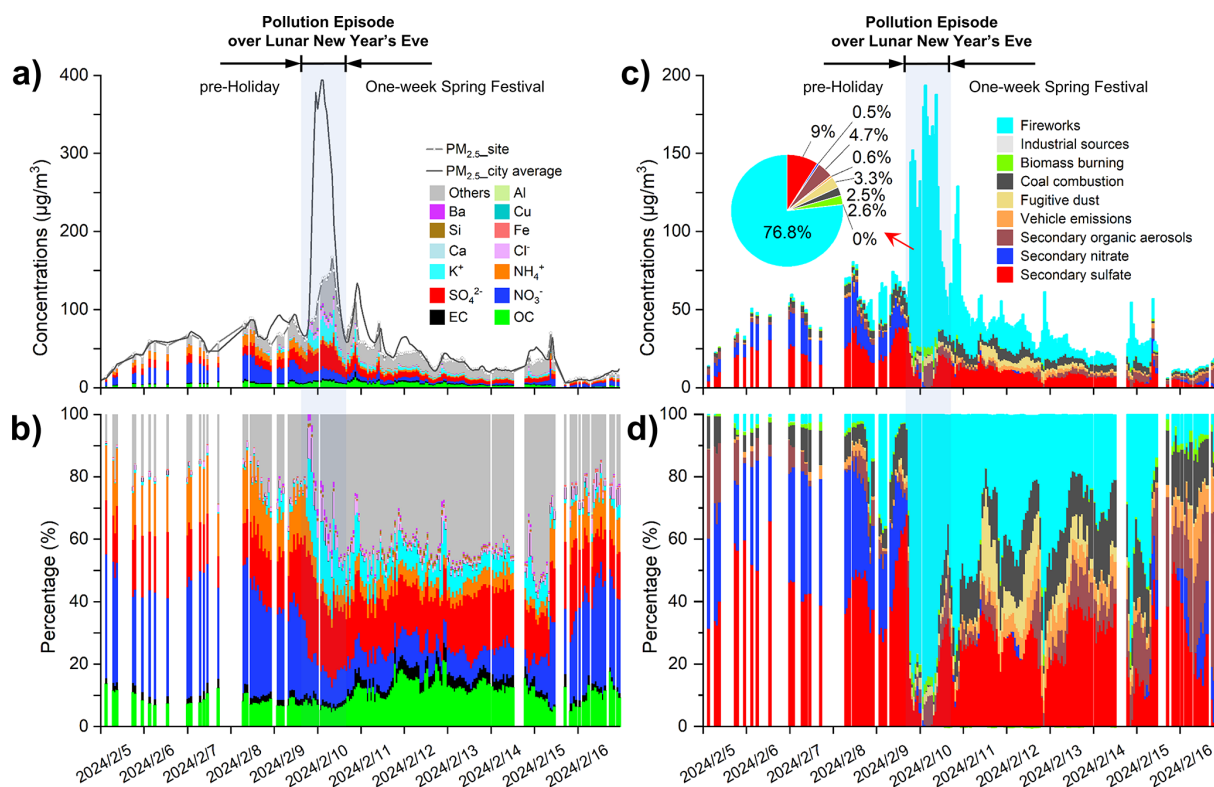


Figure 2. Changes in PM_{2.5} chemical components and source contributions throughout the CSF period. **(a)** Temporal variations of mass concentrations of PM_{2.5} chemical components. **(b)** Mass fractions of PM_{2.5} chemical components. Temporal variations of the nine PM_{2.5} sources concentrations resolved by DN-PMF **(c)** and their contribution proportions **(d)**.

previous day (from 19:00 on the 8th to 19:00 on the 9th). Particularly, fireworks emissions began to rise rapidly starting at 19:00 on the 9th, becoming the dominant emission source on New Year's Eve. They reached their peak concentration of $167.2 \mu\text{g m}^{-3}$ at 03:00 on the 10th, accounting for 88.4 % of the reconstructed PM_{2.5} (sum of speciated components) at that time. The average concentration of fugitive dust during the haze period on New Year's Eve also increased more than fivefold compared to the same period on the previous day, reaching a peak of $7.2 \mu\text{g m}^{-3}$ at 09:00 on the 10th. This significant rise may be attributed to the strong air currents generated by the ignition of fireworks, which disturbed ground-level dust and particulate matter, causing them to become re-suspended in the air and leading to a notable increase in fugitive dust concentrations. Due to reduced traffic and decreased industrial activities during the Spring Festival holiday on New Year's Eve, as well as the shutdown of local factories, emissions from motor vehicles and industrial sources experienced a rapid decline compared to the period before New Year's Eve. During the haze event on New Year's Eve, the average concentrations of vehicle emissions were only $0.3 \mu\text{g m}^{-3}$, representing an average reduction of 73 % compared with the same period on the previous day. The industrial source contribution was even lower, remaining nearly zero throughout the event. Similarly, the concentra-

tion of secondary sulfate decreased significantly during the haze event, whereas secondary organic aerosols increased. Secondary nitrate almost completely disappeared during the event. The average changes relative to the same period on the previous day were -62% , approximately -100% , and $+161 \%$, respectively.

3.3 CSF-related changes in PM_{2.5} and emission strength in Hangzhou, China

The XGBoost model trained to predict PM_{2.5} concentrations during non-pollution periods (PM_{2.5,pre}) achieved a coefficient of determination (R^2) of 0.96, a root-mean-square error (RMSE) of $7.1 \mu\text{g m}^{-3}$, and a mean absolute error (MAE) of $5.1 \mu\text{g m}^{-3}$, indicating its strong predictive performance. Excellent agreement between PM_{2.5,pre} and the observed PM_{2.5} concentrations ($R^2 = 0.98$; Fig. 3a, d) demonstrates the strong generalization ability of the model, thereby strengthening confidence in the modeled counterfactual PM_{2.5} under the *business-as-usual* (BAU) scenario during the haze period. During the pollution episode, the difference between PM_{2.5,obs} and PM_{2.5,pre} reflects the changes in PM_{2.5} air quality driven by the holiday effect, such as the emergence of fireworks and crackers emissions and the reduction in industrial and vehicle emissions. Under the com-

bined influence of these holiday-related sources change, the average PM_{2.5} air quality in Hangzhou increased by approximately 138 $\mu\text{g m}^{-3}$ (174 %), compared to the BAU scenario. The worsening air quality on the first day of the Lunar New Year was caused by both the overnight unfavorable meteorology (shallower boundary layer and smaller dilution room) and changed festival-related emissions especially the firework emissions.

The meteorological normalization random forest model demonstrated high predictive accuracy ($R^2 = 0.95$), thus can be also to normalize the meteorologically-induced variations in PM_{2.5} air quality so as to reliably reflect its emission strength changes. The holiday-driven emission strengths change can be estimated via two methods: (1) meteorologically normalization of the differences in PM_{2.5} between the real observed concentrations and the predicted BAU concentrations ($\text{PM}_{2.5, \text{emis, holiday}}$); (2) differences between the meteorologically normalized PM_{2.5} for the real observed concentrations and the predicted BAU concentrations ($\text{PM}_{2.5, \text{emis, obs-BAU}}$), with each set being normalized individually. Time series of the normalized PM_{2.5} agree with each other well ($R^2 = 0.93$, Fig. 3e), suggesting the reliability of tracking the holiday-attributable emissions using both methods following the same meteorological normalization technique. By calculating the differences between $\text{PM}_{2.5, \text{emis, obs-BAU}}$ (i.e., $\text{PM}_{2.5, \text{MN}}$ minus $\text{PM}_{2.5, \text{pred, MN}}$), the random forest models used in the meteorological normalization process for both scenarios achieved similar R^2 of approximately 0.95. These models effectively captured time series variations and produced reliable meteorologically normalized pollutant concentrations. A comparison of the time series changes in $\text{PM}_{2.5, \text{MN}}$ and $\text{PM}_{2.5, \text{pred, MN}}$ (Fig. S8) revealed that the average increase in PM_{2.5} emission strength attributable to the “holiday effect” during the pollution period was approximately 74 % (43 $\mu\text{g m}^{-3}$ in an averaged meteorological condition).

3.4 Validating CSF-attributable haze PM_{2.5} changes using source-specific data

To validate the robustness of the ML estimated CSF holiday-attributable changes in air quality and emission strength, we compare the time series of PM_{2.5} contributed by fireworks emissions, as resolved by DN-PMF, with the holiday-attributable PM_{2.5} data estimated via ML model (Fig. 3). The ML modeled holiday-attributable PM_{2.5} concentrations are overall larger than the DN-PMF-resolved fireworks contributed PM_{2.5} during the New Year’s Eve haze event. The primary reason for this discrepancy likely lies in the difference in data representativeness between the two models: one reflects a city-averaged scale, while the other is based on data from a single, albeit representative, urban site. As demonstrated by the observational data, there is an approximate 1.1-fold linear relationship between the city-averaged PM_{2.5} concentration and the PM_{2.5} data from the Wolongqiao site

(Fig. S9), meaning the city-averaged concentration is slightly larger than the site’s PM_{2.5} data. Other potential contributing factors include the complicated real-world source changes, the disproportionately strong amplification effect due to the highly unfavorable dilution conditions at midnight (e.g., extremely low VC, as shown in Fig. S1), and the inherent uncertainties associated with both methodological approaches. The fireworks emission also contributed to an increase in dust emissions. While note that the results show a high degree of temporal alignment in PM_{2.5} air quality (Fig. 3b), suggesting that the predominant role of fireworks emissions in driving holiday haze. From the perspective of emission strength changes (Fig. 3c), the “holiday effect” led to a maximum increase of 540 % in total PM_{2.5} emission strength during the Lunar New Year’s Eve haze period compared with the pre-holiday period. Concurrently, the meteorologically normalized PM_{2.5} from fireworks rose by more than 540 %, exceeding the citywide average emission increment. This indicates that the surge in fireworks emissions partially offset the reductions in industrial and vehicular emission strengths during the holiday period. The meteorologically normalized fireworks-specific PM_{2.5} explained 82 % of the overall change in PM_{2.5} emission strength during the holiday haze episode (Fig. 3f), with a positive slope of 1.2. These results suggest that, during the haze period, the holiday-related change in air quality was largely driven by shifts in festival emissions. After accounting for meteorological effects, the elevated PM_{2.5} concentrations during the holiday were predominantly attributable to firework-related source emissions. Furthermore, considering the previously established 1.1-fold linear relationship between the citywide average and site-level PM_{2.5} concentrations, the actual citywide firework emission strength is expected to be higher than the purple segment shown in Fig. 3c.

Here we acknowledge that due to the unavailability of multi-site chemical speciation data in Hangzhou, this study relies solely on speciation data from the Wolongqiao urban station. We contend that the data from this single site is sufficient and representative for validating the city-wide fireworks signal for two primary reasons. First, fireworks emissions during the CSF are not localized point sources but occur nearly simultaneously as an area-wide activity across the city. The resultant pollution plume, characterized by a sharp, synchronous peak in city-level PM_{2.5} (averaged from 14 sites), is a regional atmospheric phenomenon. Second, the Wolongqiao site’s PM_{2.5} observations demonstrate a strong positive correlation with the city-wide average (e.g., $R^2 = 0.78$, $N = 1213$). This high consistency confirms that the site’s temporal PM_{2.5} variation capture the pollution trends across Hangzhou, especially during the winter haze and Spring Festival season (Fig. S9). Additionally, the chemical fingerprint (e.g., distinct peaks in K, Ba, and the K/EC ratio) measured by the Wolongqiao site aligns perfectly with the timing of this regional PM_{2.5} peak identified by our machine learning model. This strong temporal consistency and physicochem-

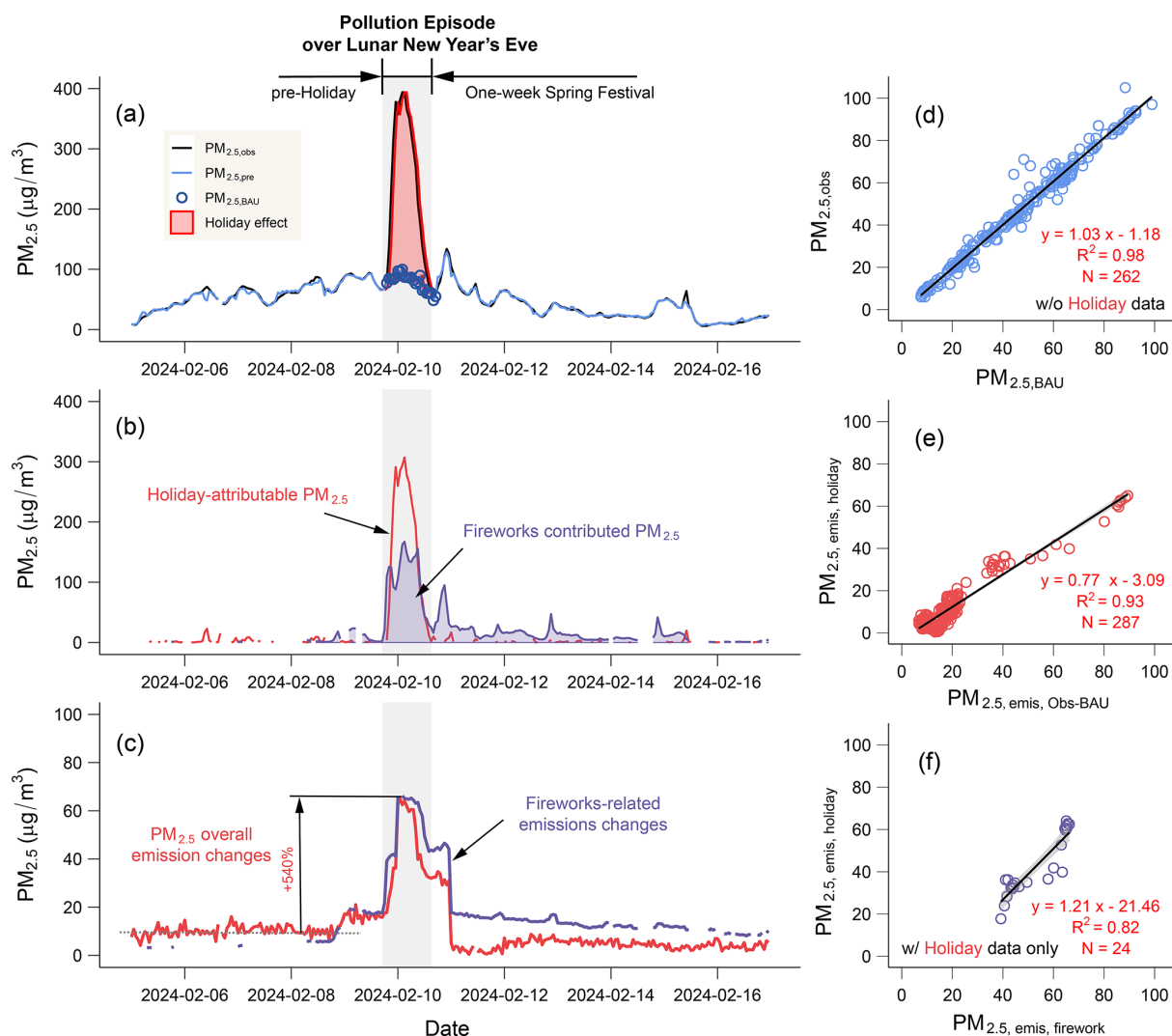


Figure 3. Changes in PM_{2.5} air quality and its emission strengths in Hangzhou around the 2024 New Year's Eve pollution period. **(a)** Temporal comparison of observed PM_{2.5} (PM_{2.5,obs}) with counterfactual predicted PM_{2.5} concentrations (PM_{2.5,BAU}). **(b)** Temporal comparison of firework-related source contributions resolved by DN-PMF with the holiday-attributable PM_{2.5} air quality changes estimated using the ML approach. **(c)** Temporal comparison between the meteorologically normalized holiday-attributable PM_{2.5} and fireworks-related PM_{2.5}. **(d)** Scatter plot for the PM_{2.5,obs} and the XGBoost model predicted PM_{2.5} concentrations (PM_{2.5,BAU}) for non-pollution periods. **(e)** Correlation between the differences in meteorologically normalized PM_{2.5,obs} and PM_{2.5,BAU} (PM_{2.5,emis,obs-BAU}) and meteorologically normalized PM_{2.5} for holiday-attributable part (PM_{2.5,emis,holiday}). **(f)** Scatter plot for the meteorologically normalized holiday-attributable PM_{2.5} and fireworks-related PM_{2.5}. Note: the PM_{2.5} concentration data were averaged from 14 national monitoring sites within Hangzhou, while the chemical composition data were measured at a single site.

ical coherence provide compelling evidence that both methods are detecting the same city-scale pollution event, thereby supporting the representativeness of the single-site chemical data for this specific analysis. Nevertheless, we acknowledge that fireworks-related tracers (e.g., K, Ba, and Cl⁻) may exhibit spatial heterogeneity due to localized burning activities. Future studies with a more extensive chemical monitoring network would be beneficial to further confirm these findings and capture potential finer-scale spatial heterogeneity.

3.5 Attribution of PM_{2.5} and emission changes to the 2025 Spring Festival in the “2 + 26” cities of northern China

Based on the validated approach, we quantified the impact of the CSF “holiday effect” on PM_{2.5} air quality and its emission strength in the Beijing-Tianjin-Hebei and surrounding “2 + 26” cities in 2025. Here we defined CSF as dates between New Year's Day to the Lantern Festival (the fifteenth day of the lunar new year). In the counterfactual prediction of PM_{2.5} air quality, the XGBoost models for the

“2 + 26” cities achieved R^2 of 0.88 ± 0.03 and RMSE of $17.7 \pm 2 \mu\text{g m}^{-3}$. The random forest meteorological normalization models for the actual observed PM_{2.5} concentrations in the “2 + 26” cities yielded R^2 of 0.89 ± 0.02 and RMSE of $19.0 \pm 2 \mu\text{g m}^{-3}$, while the meteorological normalization models for the counterfactual predicted PM_{2.5} concentrations achieved R^2 of 0.93 ± 0.02 and RMSE of $13.5 \pm 1.3 \mu\text{g m}^{-3}$. All models demonstrated strong data-fitting accuracy and robust generalization ability.

Figure 4 illustrates the impact of the 2025 CSF on PM_{2.5} levels in the “2 + 26” cities. In Fig. 4a, the regionally averaged PM_{2.5} emissions and air quality exhibit a sharp increase at the beginning of the Lunar New Year, primarily due to the intensive use of fireworks and firecrackers during New Year’s Eve celebrations, followed by a marked decline next day throughout the holiday period. This decline is attributed to reduced traffic, the suspension of construction activities, and decreased emissions from small-scale industries. Such phenomena were nearly consistently observed across all 28 cities. In Fig. 4b, a preliminary analysis was conducted to evaluate the average impact of the 2025 CSF holiday effect on PM_{2.5} air quality. The vast majority of the studied cities showed notable improvements in PM_{2.5} air quality during the nearly two weeks festival period compared to the BAU counterfactual scenario, with an average reduction of approximately $19 \mu\text{g m}^{-3}$, equivalent to a decrease of about $6 \mu\text{g m}^{-3}$ (7 %) in PM_{2.5} emission strength (in averaged meteorological condition). Among them, Puyang experienced the most significant improvement, with an average decrease of about $78.3 \mu\text{g m}^{-3}$ in PM_{2.5} concentration during the holiday. PM_{2.5} emission strength in Puyang dropped immediately after the onset of the CSF, likely due to the absence of fireworks emissions. Similar patterns were observed in Baoding, Cangzhou, and Taiyuan (Fig. S10). In contrast, even after the start of the Spring Festival, emission levels in Changzhi remained high. Baoding experienced the most severe deterioration in PM_{2.5} air quality, following by Shijiazhuang. Cities located in the central part of the “2 + 26” region showed the least improvement in air quality, which is likely attributable to increased emissions from fireworks.

The poorest air quality during the Chinese Spring Festival was observed on the first day of the Lunar New Year, coinciding with substantial midnight fireworks set off to celebrate the occasion. To quantify the contribution of firework-related emissions to the PM_{2.5} elevation on the first day, the increases in PM_{2.5} concentration relative to the counterfactual level was calculated as the lower bound of the fireworks contribution, assumption that emissions from other sources remained unchanged. In practice, pronounced reductions in other primary pollutants were observed on Chinese New Year’s Eve. NO₂ concentrations decreased from $32.8 \mu\text{g m}^{-3}$ (the average during the week preceding New Year’s Eve) to $12.2 \mu\text{g m}^{-3}$ on New Year’s Eve, corresponding to a 62.7 % reduction. Similarly, CO levels declined from 0.90 to 0.50 mg m^{-3} , representing a 44.2 % decrease

(Figs. S11 and S12). These substantial decreases in traffic- and combustion-related indicators indicate a markedly weakened background emission environment. Consequently, the fireworks contribution estimated by the counterfactual analysis should be regarded as a conservative lower bound, and is therefore likely underestimated. As shown in Fig. 5, cities experiencing severe PM_{2.5} pollution on the first day generally exhibited higher contributions from firework sources, indicating that the intensive firework displays during New Year’s Eve were a significant, and in some cities dominant, contributor to the first day haze event. On average, firework emissions accounted for at least 35 % of the PM_{2.5} concentrations across the 28 cities, with Baoding reaching a maximum of 89.2 %. Though the short-term, intensive firework emissions may offset some of the reductions achieved in other sectors, we believe that the results are reliable and can reasonably reflect the lowest contribution of firework emissions to the deterioration of PM_{2.5} air quality on the first day.

Previous studies have demonstrated that a persistent and substantial regional background pollution level exists across the “2 + 26” cities (e.g., Tiwari et al., 2025). Consistent with this established understanding, the present analysis indicates that the haze episode observed on Chinese New Year’s Eve was an acute pollution event occurring on top of this regional background. Counterfactual results suggest that this episode was primarily driven by widespread and nearly synchronous local firework emissions during the holiday period. These short-lived but intense emissions were superimposed on the prevailing background pollution, leading to a rapid deterioration in air quality on the first day.

Notably, the estimated firework contributions exhibit pronounced inter-city variability, ranging from less than 10 % to more than 80 %. This variability may be primarily controlled by differences in the prevailing background PM_{2.5} levels across cities. Because the contribution is defined relative to the total PM_{2.5} concentration, comparable firework emission intensities can result in substantially different relative contributions depending on the background pollution baseline. In cities with relatively lower regional background PM_{2.5} concentrations, short-lived but intense firework emissions during New Year’s Eve can dominate the observed PM_{2.5} enhancement, leading to very high relative contributions. In contrast, in cities characterized by persistently elevated background pollution, firework emissions contribute a smaller fraction when superimposed on an already high baseline. In addition, population redistribution during the Spring Festival, characterized by large-scale return migration from urban centers to surrounding towns and rural areas, may enhance the intensity and spatial extent of firework burning. Although firework prohibition policies are implemented at the regional scale, their effectiveness may be limited in rural areas and urban-rural fringe zones, where enforcement intensity and public compliance can differ from those in urban cores. Meteorological conditions, such as boundary layer height and atmospheric dispersion capacity during the holi-

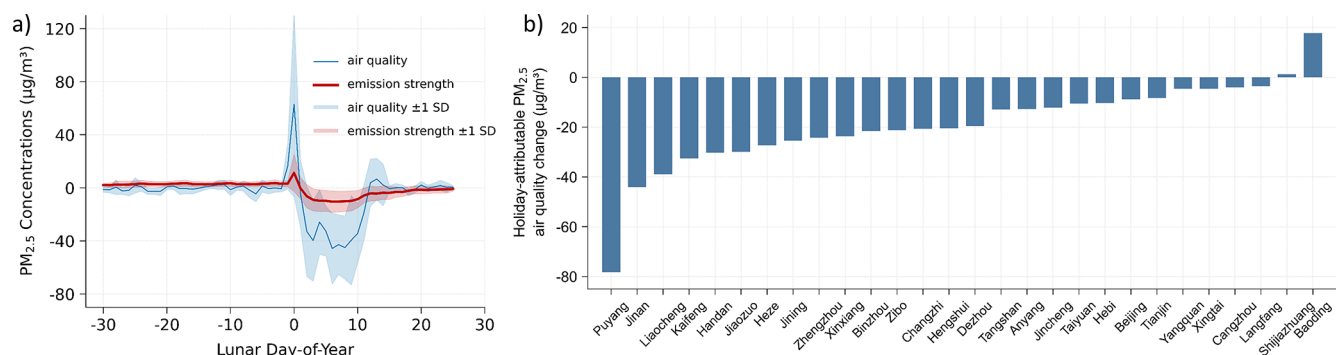


Figure 4. Impact of the 2025 CSF on PM_{2.5} in the “2 + 26” cities. **(a)** Dynamic change of regionally averaged PM_{2.5} concentrations and emission strengths during the CSF period. Shaded areas denote ±1 standard error intervals. **(b)** CSF-attributable changes in PM_{2.5} concentrations across the “2 + 26” cities, ranked by magnitude.

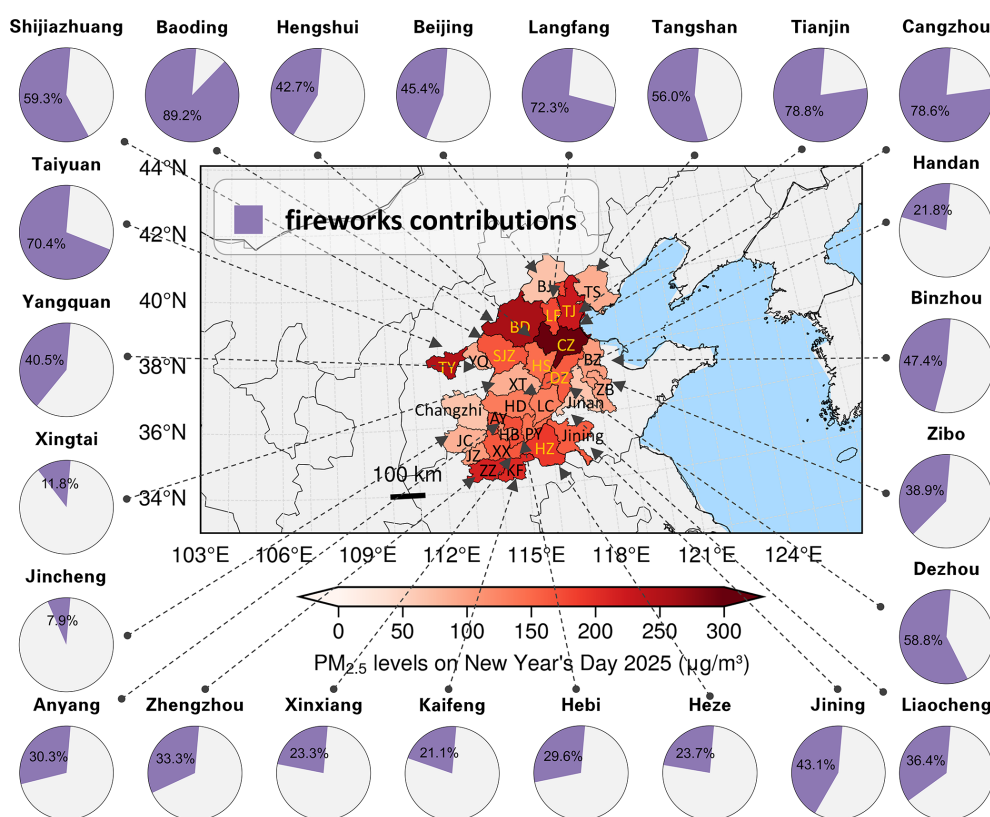


Figure 5. Holiday-related fireworks contributions to deteriorating PM_{2.5} air quality on the first day of the 2025 Lunar New Year in the “2 + 26” cities. Pie charts illustrate the city-level positive contributions of fireworks emissions to PM_{2.5} concentrations in 24 cities where air quality worsened, and the accompanying map presents the spatial distribution of observed PM_{2.5} concentrations across the region. The base maps are sourced from the Standard Map Service of the Ministry of Natural Resources of China (GS(2019)1719), providing official and authoritative geographic data. For more information, visit <http://bzdt.ch.mnr.gov.cn> (last access: 31 March 2026).

day period, may further modulate pollutant accumulation and thus the apparent contribution of firework emissions across cities.

4 Conclusions

A new machine learning-based counterfactual prediction approach was proposed to effectively estimate PM_{2.5} concentrations in the absence of Spring Festival holiday, enables us to quantify the impact of the “Spring Festival effect” on

PM_{2.5} air quality. By incorporating meteorological normalization technique, we further linked these air quality changes to variations in emission strength. The approach was applied to Beijing, Tianjin, and surrounding 26 major cities in northern China. Results demonstrate the significant contribution of holiday-related firework emissions to the elevated PM_{2.5} levels on the first day of the 2025 lunar new year in most studied cities, with average contribution over 35%. While precisely quantifying the contribution of firework emissions remains challenging, this methodology provides valuable insights into the impact of traditional Chinese festivals celebrations, such as the Spring Festival, on ambient air quality and emission strength, as well as the extent to which festive activities contribute to haze events. It also offers a promising approach for broader application in short-term air quality interventions in addition to festival-related activities.

Code and data availability. All code and data necessary for replication, including observed and meteorologically normalized air quality data, are available at Zenodo: <https://doi.org/10.5281/zenodo.19338129> (Li, 2026).

Supplement. The supplement related to this article is available online at <https://doi.org/10.5194/acp-26-5553-2026-supplement>.

Author contributions. Conceptualization – QD; Data curation and analysis – JS, RY, YL, XL, WZ, YL; Software – YL; Visualization – YL, QD; Validation – YL, WZ; Writing of original draft – YL; Review and editing of draft – QD, JD, YSL, YZ, YF; Funding acquisition and Supervision – QD, YF.

Competing interests. The contact author has declared that none of the authors has any competing interests.

Disclaimer. Publisher's note: Copernicus Publications remains neutral with regard to jurisdictional claims made in the text, published maps, institutional affiliations, or any other geographical representation in this paper. The authors bear the ultimate responsibility for providing appropriate place names. Views expressed in the text are those of the authors and do not necessarily reflect the views of the publisher.

Acknowledgements. We thank colleagues from the Hangzhou Ecological Environment Monitoring Center for providing data support. We are grateful to the support from the robotic AI-Scientist platform of Chinese Academy of Sciences.

Financial support. This work was financially supported by the National Natural Science Foundation of China (grant no. 42577117), the Young Scientific and Technological Talents

Program of Tianjin (grant no. QN20230350), the Tianjin Natural Science Foundation Project (grant no. S25YBJ077), and the Fundamental Research Funds for the Central Universities (grant no. 63251196).

Review statement. This paper was edited by Jason Cohen and reviewed by three anonymous referees.

References

- Brown, S. G., Eberly, S., Paatero, P., and Norris, G. A.: Methods for estimating uncertainty in PMF solutions: Examples with ambient air and water quality data and guidance on reporting PMF results, *Sci. Total Environ.*, 518, 626–635, <https://doi.org/10.1016/j.scitotenv.2015.01.022>, 2015.
- Dai, Q., Bi, X., Liu, B., Li, L., Ding, J., Song, W., Bi, S., Schulze, B. C., Song, C., and Wu, J.: Chemical nature of PM_{2.5} and PM₁₀ in Xi'an, China: Insights into primary emissions and secondary particle formation, *Environ. Pollut.*, 240, 155–166, <https://doi.org/10.1016/j.envpol.2018.04.111>, 2018.
- Dai, Q., Liu, B., Bi, X., Wu, J., Liang, D., Zhang, Y., Feng, Y., and Hopke, P. K.: Dispersion normalized PMF provides insights into the significant changes in source contributions to PM_{2.5} after the COVID-19 outbreak, *Environ. Sci. Technol.*, 54, 9917–9927, <https://doi.org/10.1021/acs.est.0c02776>, 2020.
- Dai, Q., Hou, L., Liu, B., Zhang, Y., Song, C., Shi, Z., Hopke, P. K., and Feng, Y.: Spring Festival and COVID-19 lockdown: disentangling PM sources in major Chinese cities, *Geophys. Res. Lett.*, 48, <https://doi.org/10.1029/2021GL093403>, 2021a.
- Dai, Q., Ding, J., Song, C., Liu, B., Bi, X., Wu, J., Zhang, Y., Feng, Y., and Hopke, P. K.: Changes in source contributions to particle number concentrations after the COVID-19 outbreak: Insights from a dispersion normalized PMF, *Sci. Total Environ.*, 759, 143548, <https://doi.org/10.1016/j.scitotenv.2020.143548>, 2021b.
- Dai, Q., Dai, T., Hou, L., Li, L., Bi, X., Zhang, Y., and Feng, Y.: Quantifying the impacts of emissions and meteorology on the interannual variations of air pollutants in major Chinese cities from 2015 to 2021, *Sci. China Earth Sci.*, 66, 1725–1737, <https://doi.org/10.1007/s11430-022-1128-1>, 2023.
- Dai, Q., Zhang, Y., Bi, X., and Feng, Y.: A Double Machine Learning Approach for Policy Evaluation Using Meteorologically Fixed Air Pollutant Time Series as an Emission Proxy, *ACS ES&T Air*, <https://doi.org/10.1021/acsestair.5c00501>, 2026.
- Ding, J., Dai, Q., Fan, W., Lu, M., Zhang, Y., Han, S., and Feng, Y.: Impacts of meteorology and precursor emission change on O₃ variation in Tianjin, China from 2015 to 2021, *J. Environ. Sci.*, 126, 506–516, <https://doi.org/10.1016/j.jes.2022.03.010>, 2023.
- Gao, J., Wang, K., Wang, Y., Liu, S., Zhu, C., Hao, J., Liu, H., Hua, S., and Tian, H.: Temporal-spatial characteristics and source apportionment of PM_{2.5} as well as its associated chemical species in the Beijing-Tianjin-Hebei region of China, *Environ. Pollut.*, 233, 714–724, <https://doi.org/10.1016/j.envpol.2017.10.123>, 2018.
- Grange, S. K., Carslaw, D. C., Lewis, A. C., Boleti, E., and Hueglin, C.: Random forest meteorological normalisation models for Swiss PM₁₀ trend analysis, *Atmos. Chem. Phys.*, 18, 6223–6239, <https://doi.org/10.5194/acp-18-6223-2018>, 2018.

- Han, B., Yao, T., Li, G., Song, Y., Zhang, Y., Dai, Q., and Yu, J.: Marginal reduction in surface NO₂ attributable to airport shutdown: A machine learning regression-based approach, *Environ. Res.*, 214, 114117, <https://doi.org/10.1016/j.envres.2022.114117>, 2022.
- Hou, L., Dai, Q., Song, C., Liu, B., Guo, F., Dai, T., Li, L., Liu, B., Bi, X., and Zhang, Y.: Revealing drivers of haze pollution by explainable machine learning, *Environ. Sci. Tech. Lett.*, 9, 112–119, <https://doi.org/10.1021/acs.estlett.1c00865>, 2022.
- Hua, J., Zhang, Y., de Foy, B., Mei, X., Shang, J., and Feng, C.: Competing PM_{2.5} and NO₂ holiday effects in the Beijing area vary locally due to differences in residential coal burning and traffic patterns, *Sci. Total Environ.*, 750, 141575, <https://doi.org/10.1016/j.scitotenv.2020.141575>, 2021.
- Huang, X., Ge, Y., Yang, T., Song, Z., Yu, S., Li, Q., Wang, X., Wang, Y., Wang, X., and Su, J.: Relaxation of spring festival firework regulations leads to a deterioration in air quality, *Environ. Sci. Technol.*, 58, 10185–10194, <https://doi.org/10.1021/acs.est.4c00920>, 2024.
- Jiang, Q., Sun, Y. L., Wang, Z., and Yin, Y.: Aerosol composition and sources during the Chinese Spring Festival: fireworks, secondary aerosol, and holiday effects, *Atmos. Chem. Phys.*, 15, 6023–6034, <https://doi.org/10.5194/acp-15-6023-2015>, 2015.
- Joshi, M., Nakhwa, A., Khandare, P., Khan, A., and Sapra, B.: Simultaneous measurements of mass, chemical compositional and number characteristics of aerosol particles emitted during fireworks, *Atmos. Environ.*, 217, 116925, <https://doi.org/10.1016/j.atmosenv.2019.116925>, 2019.
- Lai, Y. and Brimblecombe, P.: Regulatory effects on particulate pollution in the early hours of Chinese New Year, 2015, *Environ. Monit. Assess.*, 189, 1–14, <https://doi.org/10.1007/s10661-017-6167-0>, 2017.
- Lai, Y. and Brimblecombe, P.: Changes in air pollution and attitude to fireworks in Beijing, *Atmos. Environ.*, 231, 117549, <https://doi.org/10.1016/j.atmosenv.2020.117549>, 2020.
- Leist, A. K., Klee, M., Kim, J. H., Rehkopf, D. H., Bordas, S. P., Muniz-Terrera, G., and Wade, S.: Mapping of machine learning approaches for description, prediction, and causal inference in the social and health sciences, *Sci. Adv.*, 8, eabk1942, <https://doi.org/10.1126/sciadv.abk1942>, 2022.
- Li, C., van Donkelaar, A., Hammer, M. S., McDuffie, E. E., Burnett, R. T., Spadaro, J. V., Chatterjee, D., Cohen, A. J., Apte, J. S., and Southerland, V. A.: Reversal of trends in global fine particulate matter air pollution, *Nat. Commun.*, 14, 5349, <https://doi.org/10.1038/s41467-023-41086-z>, 2023.
- Li, D., Wu, Q., Wang, H., Xiao, H., Xu, Q., Wang, L., Feng, J., Yang, X., Cheng, H., and Wang, L.: The Spring Festival Effect: The change in NO₂ column concentration in China caused by the migration of human activities, *Atmos. Pollut. Res.*, 12, 101232, <https://doi.org/10.1016/j.apr.2021.101232>, 2021.
- Li, X., Cohen, J. B., Tiwari, P., Wu, L., Wang, S., He, Q., Yang, H., and Qin, K.: Space-based inversion reveals underestimated carbon monoxide emissions over Shanxi, *Commun. Earth Environ.*, 6, 357, <https://doi.org/10.1038/s43247-025-02301-5>, 2025.
- Li, Y.: Machine Learning-based Intervention Evaluation of Chinese Spring Festival Fireworks, Zenodo [data set], <https://doi.org/10.5281/zenodo.19338129>, 2026.
- Paatero, P. and Tapper, U.: Positive matrix factorization: A non-negative factor model with optimal utilization of error estimates of data values, *Environmetrics*, 5, 111–126, <https://doi.org/10.1002/env.3170050203>, 1994.
- Prosperi, M., Guo, Y., Sperrin, M., Koopman, J. S., Min, J. S., He, X., Rich, S., Wang, M., Buchan, I. E., and Bian, J.: Causal inference and counterfactual prediction in machine learning for actionable healthcare, *Nat. Mach. Intell.*, 2, 369–375, <https://doi.org/10.1038/s42256-020-0197-y>, 2020.
- Pui, D. Y., Chen, S.-C., and Zuo, Z.: PM_{2.5} in China: Measurements, sources, visibility and health effects, and mitigation, *Particuology*, 13, 1–26, <https://doi.org/10.1016/j.partic.2013.11.001>, 2014.
- Pye, H. O., Ward-Caviness, C. K., Murphy, B. N., Appel, K. W., and Seltzer, K. M.: Secondary organic aerosol association with cardiorespiratory disease mortality in the United States, *Nat. Commun.*, 12, 7215, <https://doi.org/10.1038/s41467-021-27484-1>, 2021.
- Shi, Z., Song, C., Liu, B., Lu, G., Xu, J., Van Vu, T., Elliott, R. J., Li, W., Bloss, W. J., and Harrison, R. M.: Abrupt but smaller than expected changes in surface air quality attributable to COVID-19 lockdowns, *Sci. Adv.*, 7, eabd6696, <https://doi.org/10.1126/sciadv.abd6696>, 2021.
- Tian, Y. Z., Wang, J., Peng, X., Shi, G. L., and Feng, Y. C.: Estimation of the direct and indirect impacts of fireworks on the physicochemical characteristics of atmospheric PM₁₀ and PM_{2.5}, *Atmos. Chem. Phys.*, 14, 9469–9479, <https://doi.org/10.5194/acp-14-9469-2014>, 2014.
- Tiwari, P., Cohen, J. B., Lu, L., Wang, S., Li, X., Guan, L., Liu, Z., Li, Z., and Qin, K.: Multi-platform observations and constraints reveal overlooked urban sources of black carbon in Xuzhou and Dhaka, *Commun. Earth Environ.*, 6, 38, <https://doi.org/10.1038/s43247-025-02012-x>, 2025.
- Viana, M., Kuhlbusch, T. A., Querol, X., Alastuey, A., Harrison, R. M., Hopke, P. K., Winiwarter, W., Vallius, M., Szidat, S., and Prévôt, A. S.: Source apportionment of particulate matter in Europe: a review of methods and results, *J. Aerosol Sci.*, 39, 827–849, <https://doi.org/10.1016/j.jaerosci.2008.05.007>, 2008.
- Vu, T. V., Shi, Z., Cheng, J., Zhang, Q., He, K., Wang, S., and Harrison, R. M.: Assessing the impact of clean air action on air quality trends in Beijing using a machine learning technique, *Atmos. Chem. Phys.*, 19, 11303–11314, <https://doi.org/10.5194/acp-19-11303-2019>, 2019.
- Wang, W., Zhou, H., Gao, Y., Shao, L., Zhou, X., Li, X., Wei, D., Xing, J., and Lyu, R.: Chemical composition and morphology of PM_{2.5} in a rural valley during Chinese New Year's Eve: Impact of firework/firecracker display, *Atmos. Environ.*, 318, 120225, <https://doi.org/10.1016/j.atmosenv.2023.120225>, 2024.
- Wang, Y., Zhuang, G., Xu, C., and An, Z.: The air pollution caused by the burning of fireworks during the lantern festival in Beijing, *Atmos. Environ.*, 41, 417–431, <https://doi.org/10.1016/j.atmosenv.2006.07.043>, 2007.
- Wei, P., Xie, S., Huang, L., Liu, L., Tang, Y., Zhang, Y., Wu, H., Xue, Z., and Ren, D.: Spatial interpolation of PM_{2.5} concentrations during holidays in south-central China considering multiple factors, *Atmos. Pollut. Res.*, 13, 101480, <https://doi.org/10.1016/j.apr.2022.101480>, 2022.
- Wu, G., Tian, W., Zhang, L., and Yang, H.: The Chinese spring festival impact on air quality in China: A critical review, *Int. J. Env. Res. Pub. He.*, 19, 9074, <https://doi.org/10.3390/ijerph19159074>, 2022.

- Yang, J., Zhou, M., Li, M., Yin, P., Hu, J., Zhang, C., Wang, H., Liu, Q., and Wang, B.: Fine particulate matter constituents and cause-specific mortality in China: a nationwide modelling study, *Environ. Int.*, 143, 105927, <https://doi.org/10.1016/j.envint.2020.105927>, 2020.
- Yang, T., Liu, B., Yang, Y., Dai, Q., Zhang, Y., Feng, Y., and Hopke, P. K.: Improved positive matrix factorization for source apportionment of volatile organic compounds in vehicular emissions during the Spring Festival in Tianjin, China, *Environ. Pollut.*, 303, 119122, <https://doi.org/10.1016/j.envint.2021.106979>, 2022.
- Yin, X., Sun, Z., Miao, S., Yan, Q., Wang, Z., Shi, G., Li, Z., and Xu, W.: Analysis of abrupt changes in the PM_{2.5} concentration in Beijing during the conversion period from the summer to winter half-year in 2006–2015, *Atmos. Environ.*, 200, 319–328, <https://doi.org/10.1016/j.atmosenv.2018.11.057>, 2019.
- Zhou, W., Xu, W., Wang, Q., Li, Y., Lei, L., Yang, Y., Zhang, Z., Fu, P., Wang, Z., and Sun, Y.: Machine learning elucidates the impact of short-term emission changes on air pollution in Beijing, *Atmos. Environ.*, 283, 119192, <https://doi.org/10.1016/j.atmosenv.2022.119192>, 2022.